Chemical Speciation & Bioavailability

ISSN: 0954-2299 (Print) 2047-6523 (Online) Journal homepage: https://www.tandfonline.com/loi/tcsb20

Scavenging Rhodamine B dye using *moringa oleifera* seed pod

Olugbenga Solomon Bello, Bukola Morenike Lasisi, Olamide Joshua Adigun & Vunain Ephraim

To cite this article: Olugbenga Solomon Bello, Bukola Morenike Lasisi, Olamide Joshua Adigun & Vunain Ephraim (2017) Scavenging Rhodamine B dye using *moringa oleifera* seed pod, Chemical Speciation & Bioavailability, 29:1, 120-134, DOI: 10.1080/09542299.2017.1356694

To link to this article: https://doi.org/10.1080/09542299.2017.1356694

Published online: 25 Jul 2017.

CHEMICAL SPECIATION & BIOAVAILABILITY, 2017
VOL. 29, NO. 1, 120–134
https://doi.org/10.1080/09542299.2017.1356694

Taylor & Francis
Taylor & Francis Group

Scavenging Rhodamine B dye using *moringa oleifera* seed pod

Olugbenga Solomon Bello[a], Bukola Morenike Lasisi[a], Olamide Joshua Adigun[a] and Vunain Ephraim[b]

[a]Department of Pure and Applied Chemistry, Ladoke Akintola University of Technology, Ogbomoso, Nigeria; [b]Chancellor College, University of Malawi, Zomba, Malawi

ABSTRACT

Moringa oliferia seed pod was modified using orthophosphoric acid (H_3PO_4) and used as adsorbent for sequestering Rhodamine B (Rh-B) dye from aqueous solution. The acid-modified adsorbent (MOSPAC) was characterized using Scanning Electron microscopy (SEM), Fourier Transform Infra Red (FTIR), Energy Dispersive X-ray (EDX), pH point of zero charge (pH_{pzc}) and Boehm Titration (BT) techniques, respectively. Operational parameters such as contact time, initial dye concentration, adsorbent dosage, pH and solution temperature were studied in batch process. Optimum dye adsorption was observed at pH 3.01. Equilibrium adsorption data was tested data using four different isotherm models: Langmuir, Freundlich, Temkin and Dubinin-Radushkevich. Langmuir isotherm model fitted most with maximum monolayer adsorption capacity of 1250 mg g^{-1}. Pseudo-second-order kinetic model provided the best correlation for the experimental data. Thermodynamic study showed that the process is endothermic, spontaneous and feasible. MOSPAC is an effective adsorbent for the removal of RhB dye from aqueous solutions.

ARTICLE HISTORY
Received 29 March 2017
Accepted 12 July 2017

KEYWORDS
Adsorption; Rhodamine B; moringa seed pod; kinetics; thermodynamics

Introduction

Color is a visible pollutant and one of the most important substance found in industrial effluents. The presence of dyes and pigments in water, even in very low concentrations, is highly undesirable [1]. Textile, pharmaceutical, paper and plastic industries generate large volumes of colored wastewater mostly resulting from the dye preparation, spent dye, bath and washing stages. Textile industries generate vast volume of wastewater. It contains a number of contaminants including suspended solids, acidic or caustic, dissolved solids, sulfite, chromium, lime, organic solids, toxic compounds, and different types of dyes. Their presence in water bodies restricts light penetration thereby reducing photosynthetic activity [2]. Thus, water pollution is a highly undesirable cause of ecological problems which needs attention. Pollutants make water unsuitable for drinking. Discharge of dye-colored water into water bodies causes allergy, dermatitis, skin irritation, and could in extreme cases, provoke cancer and mutation in humans [3]. Furthermore, the color and non-biodegradable nature of the spent dye baths constitute serious environmental problems.

Rhodamine B (Rh-B) is a basic dye, which is widely used in textile, trace, biological laboratory purposes etc. It is a red dye used to dye wool, silk and tannin mordant cotton. Effluents containing Rh-B are generated from a number of industrial activities such as textile, printing and dyeing processes, paper manufacturing, rubber and plastic production, production of biological stains, etc. In addition to its application in dyeing industries, Rh-B in combination with Uramine-O (a basic dye) is used as a biological stain widely used in biomedical research laboratories as well as in the dyeing of leather and paper. Various techniques, such as adsorption [4], coagulation/flocculation [5,6], photocatalytic processes [7,8], membrane technology [9,10] and biological treatments [11,12] have been employed to remove dyes from wastewater. Other conventional methods employed in removing dyes include oxidation or ozonation and membrane separation. However, these methods are not widely used due to their expensive costs. Chemical, electrochemical oxidation and coagulation are generally not feasible for large scale industries. Adsorption techniques for treatment of effluents have become widely used due to their higher efficiency in removing pollutants as compared to biological methods. Adsorption has great potential for effluent treatment because it converts effluents to both safe and reusable forms [13].

The most widely used adsorbent in industrial scale for effluent treatment is activated carbon. As documented in

CONTACT Olugbenga Solomon Bello osbello@lautech.edu.ng

other studies, the use of activated carbon in the removal of dyes is effective and technically easier. Activated carbon has high surface area and a microporous structure, which contributes to a high adsorption capacity. These properties confer on it wide usage as an adsorbent. However, there are certain drawbacks associated with its use especially the expensive nature of high quality activated carbon. As such, there has been an increase in research into cheaper and more readily available adsorbents [14]. Some of the non-conventional, low cost adsorbents that have been utilized for the removal of dyes and other pollutants from wastewater include durian seed [15,16], mango leaf [17], wheat husk [18], coconut shell [19], periwinkle shell [20], Indian spinach leaf, bottom ash and de-oiled soya [21–23], brown linseed deoiled cake [24], waste tyre[25], native and citric acid modified bamboo sawdust [26], chir pine (*Pinus roxburghii*) sawdust [27], magnetic chitosan-bamboo sawdust composite [28], Multiwalled carbon nanotube–polyurethane (MWCNT/PU) composite [29], Magnetically modified multiwalled carbon nanotubes [30], magnesium oxide-coated kaolinite [31].

Moringa seed pod husks are a bountiful low-cost source of activated carbon. Unlike other sources of activated carbon that requires extensive processing prior to use, moringa seed pods can be processed using single-step steam pyrolysis, a simple method that can be performed even in remote areas and without advanced technological tools. This study is focused on converting *moringa oleifera* seed pods into activated carbon and testing its efficiency in the removal of Rh-B dye from aqueous solutions. Rh-B was selected for the adsorption experiment due to its presence in the wastewaters of several industries (such as textile, leather, jute and food industries). The effects of operational factors such as the initial dye concentration, adsorbent dosage, pH study, contact time, and temperature were investigated. The kinetics of Rh-B dye adsorption was analyzed by fitting to four different isotherm equations: Langmuir, Freundlich, Temkin, and D-R isotherms. Four different kinetic model equations namely pseudo-first-order, pseudo-second-order, Elovich and intraparticle diffusion models were also used to fit the adsorption data.

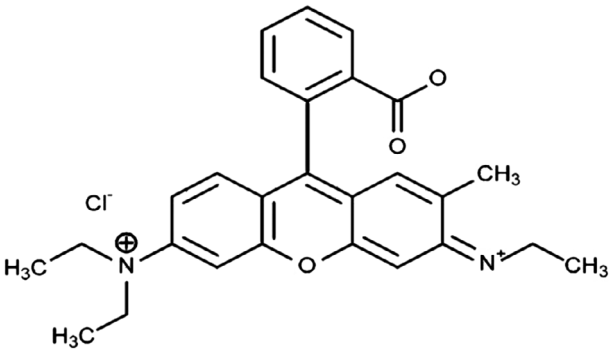

Figure 1. Structure of Rhodamine-B dye.

Materials and methods

Sample collection and pre-treatment

Moringa seed pod were collected from local agricultural field in Ogbomoso, Oyo State. Nigeria, washed with distilled water and dried to constant weight. Thereafter, the seed pods were ground, then sieved to a size of 106 µm. It was then dried using a hot air oven at 105 °C for 6 h. Finally, it was stored in vacuum desiccators.

Activated carbon preparation

A carefully weighed 30.0 g of the prepared adsorbent was placed in a beaker containing 600 cm^3 of 0.3 mol/dm^3 ortho-phosphoric acid (H_3PO_4). The content of the beaker was thoroughly mixed and heated until it formed a paste. It was then transferred to an evaporating dish which was placed in the furnace and heated to 300 °C for 30 min. This was allowed to cool and washed with distilled water to maintain a pH of 6.8, oven dried at 105 °C for 6 h to constant weight and then ground. It was sieved with 106 µm mesh size to obtain fine powdered Moringa seed pod activated carbon (MOSPAC) which was kept in an air-tight container and used for various experiments.

Adsorbate used

All chemicals used for this experiment are of analytical grade. Rhodamine B (Rh-B) dye was used as adsorbate to determine the adsorption performance of the prepared activated carbon from moringa seed pod. It has the following properties: C.I Number: 45170, C.I Name: Basic Violet 10, Class: Rhodamine, λ_{max}: 554 nm, Molecular formula: $C_{28}H_{31}N_2O_3Cl$, Formula weight: 497.02 g/mol. The chemical structure of Rh-B dye is shown in Figure 1.

Preparation of dye solution

1000 mg/L of dye solution was prepared by dissolving 1.0 g of Rh-B dye powder in 1000 ml of distilled water. Different dilutions, ranging from 200 to 1000 mg/L, were then prepared by serial dilution using distilled water.

Adsorption experiments

Adsorption of Rh-B dye on MOSPAC was carried out using batch method at 30, 40 and 50 °C respectively. Effects of the initial dye concentration, contact time, adsorbent dosage, pH and solution temperature were investigated. The adsorption process was carried out at five different initial dye concentrations at 200, 400, 600, 800, and 1000 mg/L. 0.1 g of adsorbent was weighed in 200 mL Erlenmeyer flask. Hundred milliliter of Rh-B dye solution was added to the flask. Sample solutions were withdrawn

at pre-determined time intervals after shaking in a water bath shaker at 150 rpm to determine the percentage Rh-B dye removed from the solution. The residual concentrations of the dye solutions were calculated by measuring the absorbance at a wavelength of 554 nm with UV-Visible spectrophotometer. The amount of Rh-B dye adsorbed was calculated by:

$$q_e = \frac{(C_0 - C_e)V}{w} \tag{1}$$

where q_e is the amount of dye adsorbed by the activated carbon, C_0 is the initial equilibrium concentration of adsorbate, and C_e is the equilibrium concentration of dye solution, w is the mass of the adsorbent in grams (g) and V is the initial volume of dye solution used in dm^3.

Adsorption isotherm studies

This was carried out by fitting the equilibrium data to four different isotherms namely: Langmuir, Freundlich, Temkin, and Dubinin-Radushkevich isotherms respectively.

Langmuir isotherm

This model assumes that intermolecular forces decrease rapidly with distance. It helps to predict the existence of monolayer coverage of the adsorbate on the outer surface of adsorbent. The Langmuir isotherm equation [32] is given by:

$$\frac{C_e}{q_e} = \frac{1}{q_m}C_e + \frac{1}{K_L q_m} \tag{2}$$

C_e is the equilibrium concentration of adsorbate (mg/L), C_0 is the initial concentration of adsorbate (mg/L), q_e is the amount of adsorbate adsorbed per unit mass of adsorbent (mg/g), q_m is the monolayer adsorption capacity of the adsorbent (mg/g), b is the Langmuir adsorption constant (L/mg). A graphical plot of C_e/q_e against C_e will give a straight line with slope of $1/q_m$ and intercept of $1/K_L q_m$. Further analysis of the Langmuir equation was made using a dimensionless equilibrium parameter, R_L also known as the separation factor, given by:

$$R_L = \frac{1}{(1 + K_L C_0)} \tag{3}$$

where; C_0 is the highest initial solute concentration (mg/L), K_L is the Langmuir adsorption constant related to the free energy of adsorption (L/mg).

Freundlich isotherm

The Freundlich isotherm assumes that the adsorption of ions occurs on a heterogeneous medium through multilayer means and that the amount of adsorbate adsorbed increases infinitely with an increase in concentration. It is the most popular model for a single solute system. It is based on the equilibrium distribution of molecules of solute between the solid and aqueous phase. It can be expressed as [33]:

$$q_e = K_f C_e^{1/n} \tag{4}$$

It can then be further rearranged to:

$$\log q_e = \frac{1}{n}\log C_e + \log K_f \tag{5}$$

q_e is the amount of adsorbate adsorbed per unit mass of adsorbent (mg/g), $1/n$ is the adsorption intensity, C_e is the equilibrium concentration of the adsorbate (mg/L), K_f and n are Freundlich constant related to the adsorption capacity and adsorption intensity respectively. A plot of log q_e vs. log C_e gives a slope of $1/n$ with intercept of log K_f. The slope of the graph normally ranges from 0 to 1. When the value is close to 0, it indicates that the system is more heterogeneous. Meanwhile, with the value lower that 1, it shows a normal Langmuir isotherm. While, when the value is above 1, it shows that the system has cooperative adsorption. K_f is a constant related to the binding energy of a system. It is the adsorption or distribution coefficient that represents the quantity of dye adsorbed onto the adsorbent at a unit equilibrium concentration (i.e. when $C_e = 1$ mg/dm^3).

Temkin isotherm

The Temkin isotherm model [34] has been developed on the concept of chemisorption. It assumes that the heat of adsorption of the molecules of the adsorbate linearly decreases with adsorbent layer coverage due to adsorbate-adsorbent interactions. The Temkin model can be expressed as [30]:

$$q_e = B\ln(K_T C_e) \tag{6}$$

This can then be further rearranged to:

$$q_e = B\ln K_T + B\ln C_e \tag{7}$$

where: q_e is the amount of adsorbate adsorbed at equilibrium (mg/g), $B = RT/b$ = Constant related to the heat capacity (L/mg), R is the Universal gas constant (8.314 J/mol K), T is the absolute temperature (K), K_T is the equilibrium binding constant (L/mg), C_e is the equilibrium concentration of adsorbate (mg/L).

Dubinin-Radushkevich isotherm

The Dubinin-Radushkevich is expressed as [35]:

$$q_e = q_m \exp\left(-B\varepsilon^2\right) \tag{8}$$

where:

$$\varepsilon = RT\ln\left[1 + \frac{1}{C_e}\right] \tag{9}$$

where: q_e is the amount of adsorbate adsorbed at equilibrium, q_m is the maximum adsorption capacity.

B is the Dubinin-Radushkevich constant, R is the universal gas constant, T is the absolute solution temperature, C_e is the equilibrium concentration of adsorbate. Therefore, a graph of ln q_e against ε^2 will give a straight line with slope of B and intercept of ln q_m. Also, from the value of B, the free energy of sorption per molecule of the adsorbate, E, can be determined by using the equation:

$$E = \frac{1}{\sqrt{2B}} \tag{10}$$

The adsorption energy E helps in determining the nature of adsorption. The adsorption is physical if E ranges from 1 to 8 kJ/mol. If the value of E ranged between 9 and 16 kJ/mol, it is chemical adsorption [36].

Adsorption kinetic studies

Kinetic study provides valuable information on the reaction pathways as well as the mechanism of the reaction. It relates the relationship between adsorption rate and concentration of adsorbate in the solution besides determining how the adsorption rate is affected by the adsorption capacity. Four kinetic models were used to test the adsorption data; they are pseudo-first-order, pseudo-second-order, Elovich and intraparticle diffusion models, respectively.

Pseudo-first order kinetic model

The pseudo-first order kinetic model is the earliest equation used to describe adsorption rate based on adsorption capacity. The model assumes that the rate of change of adsorption of solute with time is proportional to the difference in saturation concentration and the amount of solid uptake with time. It is generally expressed as [37]:

$$\ln\left(q_e - q_t\right) = \ln q_e - k_1 t \tag{11}$$

The values of k_1 and q_e can be obtained from the slope and intercept of the linear plot of ln $(q_e - q_t)$ vs. t.

Pseudo-second order kinetic model

The pseudo-second order kinetic model is based on the adsorption capacity onto a solid phase. It is used to predict the behaviour over the entire range studied. It can be expressed as [38]:

$$\frac{t}{q_t} = \frac{1}{k_2 q_e^2} + \frac{1}{q_e} t \tag{12}$$

The slope and intercept of the plot of t/q_t vs. t give the values of q_e and k_2, respectively.

If the initial adsorption rate, h (mg g^{-1} min^{-1}) is

$$h = k_2 q_e^2 \tag{13}$$

Plots of t/q_t vs. t gave linear graphs from which q_e and k_2 were estimated from the slopes and intercepts of the plot for temperatures 30–60 °C.

Test of kinetic models

Besides the value of R^2, the applicability of both kinetic models are verified through the sum of error squares (SSE, %). The adsorption kinetics of Rh-B onto MOSPAC was tested at different initial concentrations. The validity of each model was determined by the sum or error squares (SSE, %) given by:

$$\mathrm{SSE}(\%) = \sqrt{\sum \left(\frac{q_{e,\mathrm{exp}} - q_{e,\mathrm{calc}}}{N}\right)^2} \tag{14}$$

where: N is the number of data points. The higher is the value of R^2 and the lower is the value of SSE; the better is the goodness of fit.

Elovich kinetic model

The Elovich equation is suitable in describing the kinetics of adsorption on heterogeneous solids. The Elovich model is expressed by the following equation [39]:

$$q_t = \left(\frac{1}{\beta}\right) \ln(\alpha\beta) + \frac{1}{\beta} \ln t \tag{15}$$

where: α is the initial sorption rate (mg/g min), β is the extent of surface coverage and activation energy for chemisorption (g/mg), The slope and intercept of the plot of q_t vs. ln t can be used to calculate the values of the constants α and β respectively.

Intraparticle diffusion model

The adsorption process is generally made up of a series of steps. The steps include: transport of adsorbate from the boundary film to the external surface of the adsorbent; adsorbate at a site on the surface; Intraparticle diffusion of the adsorbate molecules. The slowest of the three steps controls the overall rate of the process. In the intraparticle diffusion model, the uptake varies almost proportional to $t^{1/2}$. It can be expressed as [40]:

$$q_t = k_{\mathrm{diff}} t^{1/2} + C \tag{16}$$

where: q_t is the amount of the adsorbate adsorbed at time t, k_{diff} is the intraparticle diffusion rate constant (mg/g min$^{1/2}$), C is the intercept, Therefore, a graph of q_t against $t^{1/2}$ will give a straight line with the slope of k_{diff} and intercept of C. The intercept of the plot reflects the boundary layer effect. The contribution of the surface sorption in the rate-controlling step depends on the value of the intercept. Also, if the plot of q_t vs. $t^{1/2}$ is linear and passes through the origin of the plot, then only the intraparticle diffusion model can be considered as the rate-limiting step. Otherwise, it indicates that there

are some other mechanisms that are involved along with intraparticle diffusion.

Thermodynamic studies

Thermodynamic parameters are used to reveal the energy changes that occur in an adsorption process. In order to investigate the adsorption process, three thermodynamic parameters were evaluated. They include: Standard enthalpy change (ΔH^o), Standard entropy change (ΔS^o); and Standard free energy change (ΔG^o). These values can be calculated by using the following equation:

$$\ln K_L = \frac{\Delta S^o}{R} - \frac{\Delta H^o}{RT} \tag{17}$$

where: K_L is the Langmuir adsorption constant (L/mg), ΔS^o is the change in standard entropy (kJ/mol K), R is the Universal gas constant (8.314 J/mol K), ΔH^o is the change in standard enthalpy (kJ/mol K). T is the absolute solution temperature (K), Hence, a plot of ln K_L against $1/T$ yields the values of both ΔH^o and ΔS^o from the slope and intercept of the graph respectively. Fundamentally, a positive ΔH^o value indicates that an adsorption process is endothermic in nature while a negative value represents exothermic reaction. A positive value of ΔS^o signifies an increase in randomness at the solid/solution interface that occurs in the adsorption process besides reflecting the affinity of the adsorbent toward the adsorbate [41]. Furthermore, a negative ΔG^o value indicates that an adsorption process is a spontaneous process at the study temperature and vice versa. ΔG^o can be calculated using the following relation:

$$\Delta G^o = -RT \ln K_L \tag{18}$$

As the nature of adsorption is determined by the magnitude of activation energy, E_a, the Arrhenius equation was applied to determine whether the process is physical or chemical. The physisorption process has activation energy ranging between 5 and 40 kJ/mol. If the adsorption is a chemisorption process, the activation energy is higher and ranges from 40 to 800 kJ/mol [42].

Arrhenius equation is represented by:

$$\ln k_2 = \ln A - \frac{E_a}{RT} \tag{19}$$

where: K_2 is the the rate constant obtained from the pseudo-second order kinetic model (g/mg min). A is the Arrhenius factor E_a is the Arrhenius activation energy of adsorption (kJ/mol). R is the universal gas constant (8.314 J/mol K), T is the absolute temperature (K). Therefore, a plot of ln K_2 against $1/T$ is expected to give a straight line. The value of E_a can be obtained from the slope of the graph.

Characterization of adsorbents

Scanning electron microscopy (SEM)

The Scanning Electron Microscopy (SEM) is a technique based on electron-material interactions, capable of producing images of the sample surface. The principle of the SEM is based on the fact that an electron beam bombards the surface of the sample to be analyzed which re-emits certain particles. These particles are analyzed by various detectors which give a three dimensions image of the surface. This technique was used to study the morphological feature and surface characteristics of the prepared adsorbents.

Fourier transform infrared (FTIR)

Fourier Transform Infrared (FTIR) spectroscopic analysis was used to study the surface chemistry of raw and activated carbon prepared from moringa seed pod samples using FTIR (FTIR-2000, Perkin Elmer). The FTIR spectral gave the information about the characteristics functional groups on the surface of these adsorbents.

Energy dispersive X-ray (EDX)

Elemental analyses were carried out using EDX, it determine the component elements present in both raw and activated MOSP. Line spectra (peaks) are obtained, each corresponding to a particular element. The intensity of the characteristic lines is proportional to the concentration of the element.

Determination of point of zero charge (pH_{pzc})

The pH point of zero charge determination (pH_{pzc}) of both raw and activated MOSP were carried out by adding 0.1 g of activated carbon to 200 ml solution of 0.1 M NaCl whose initial pH has been measured and adjusted with NaOH or HCl. The containers were sealed and placed on a shaker for 24 h after which the pH was measured. The pH_{pzc} occurs when there is no change in the pH after contact with adsorbent.

Determination of oxygen containing functional groups

The Boehm titration method was used for this analysis [43]. One gram of the raw and the activated MOSP were kept in contact with 15 ml solution of $NaHCO_3$ (0.1 M), Na_2CO_3 (0.05 M) and NaOH (0.1 M) for acidic group and 0.1 HCl for basic group/site respectively at room temperature for more than 2 days. Subsequently, the aqueous solution were back titrated with HCl (0.1 M) for acid and NaOH (0.1 M) for basic groups. The number and type of acidic site were calculated by considering that NaOH neutralises carboxylic, lactonic and phenolic groups, Na_2CO_3 neutralises carboxylic and lactonic groups and that $NaHCO_3$ neutralises only carboxylic groups. The amount of oxygen containing functional groups, F_x, is calculated as follows:

$$F_x = \frac{(V_{bx} - V_{ex})}{m_x} \times M_t \times \mathrm{DF} \quad (20)$$

$$\mathrm{DF} = \frac{\text{initial volume}}{\text{selected volume for titration}} \quad (21)$$

Where F_x (mmolg^{-1}) is the amount of oxygen containing functional groups, V_{bx} is the volume of titrant used to titrate the blank, V_{ex} is the volume of the titrant used to titrate the extract, M_t is the molarity of the titrant used and DF is the dilution factor.

Results and discussion

Characterization of moringa seed pod adsorbent

Scanning electron microscopy (SEM)

Scanning electron microscopy (SEM) was used to demonstrate the surface morphology of MOSPAC. Figure 2(a) and (b) show the SEM micrographs of raw MOSP and MOSPAC respectively. The surface structures of the raw sample were not well developed, however, for MOSPAC, lots of pores were observed as a result of the modification of the adsorbent using H_3PO_4 as the activating agent. A significant pore structure exists with a series of rough cavities distributed over the surface of the adsorbents. This was due to the breakdown of the lignocellulosic material at high temperature followed by evaporation of volatile compounds leaving samples with well-developed pores. These pores provided a good surface for the Rh-B dye to be adsorbed into [44]. During activation process, the C–H_3PO_4 reaction rate was increased. This resulted in carbon 'burn off' thereby developing large pores on the sample. The C–H_3PO_4 reaction also increased the porosity of the adsorbents as well as creating new pores due to loss of volatile components in the form of CO and CO_2 [45]. The physiochemical treatment was able to produce porous adsorbent thereby increasing the surface area. The activation process had resulted in enhancement of porous structure of the adsorbent.

Fourier transform infrared spectroscopy (FTIR)

In order to investigate the surface chemistry of the sample, Fourier Transform Infrared Spectroscopy (FTIR) analysis was carried out to reveal the presence of several peaks or functional groups. The FTIR spectra of the adsorbent before and after activation are shown in Figure 3(a) and (b) respectively. The figure reveals that some peaks are shifted, disappeared and some new peaks are also detected which may be due to the activation process. Similarly, FTIR data of the *moringa olifera* seed pod adsorbent are shown in Table 1. Similar observations have been reported by other researchers. Lim and co workers observed the disappearance and appearance of several peaks in their study on the adsorption of toxic Rhodamine B on *Artocarpus odoratissimus* peel [46]. Similarly, in a study conducted by Muhammad and other investigators, shifts in FTIR bands are observed in their study conducted on remediation of Rhodamine B dye from aqueous solution using *Casuarina equisetifolia* cone powder as a low cost adsorbent [47].

Energy-dispersive X-ray (EDX) technique

The elemental composition of the *moringa olifera* seed pod adsorbent before and after adsorption was also studied using the Energy-Dispersive X-ray (EDX) technique.

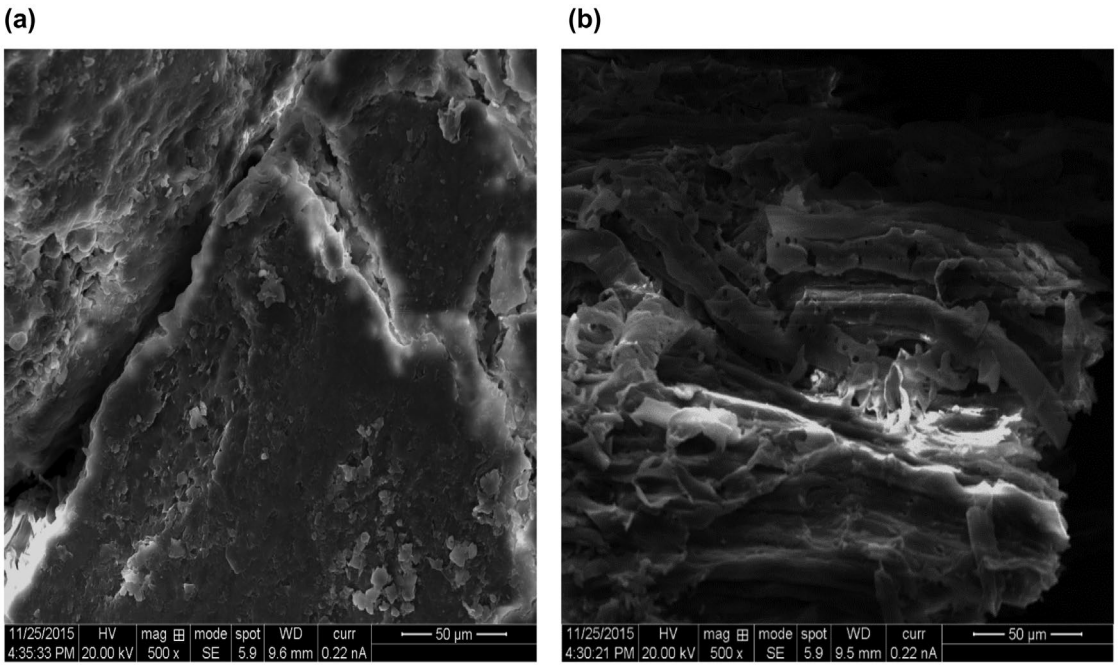

Figure 2. SEM micrograph of (a) MOSPR and (b) MOSPAC (magnification = 500×).

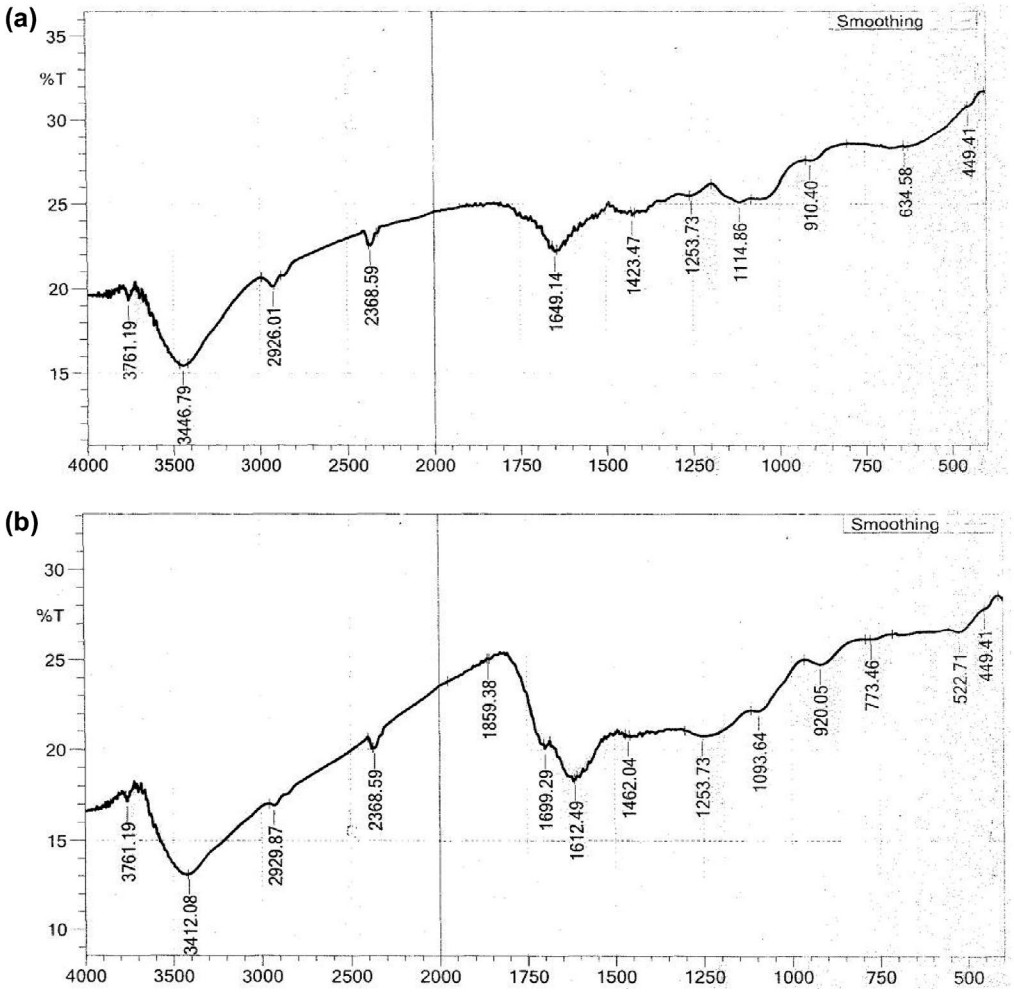

Figure 3. FTIR spectrum of (a) MOSPR and (b) MOSPAC.

Table 1. FTIR spectra characteristics of raw and acid activated moringa olifera seed pod (MOSP).

	Wave numbers (cm^{-1})			
I.R peaks	MOSPR	MOSPAC	Differences	Band assignments
1	3447	3412	−35	O–H stretching, H-bonding of alcoholic phenols
2	2926	2930	4	C–H stretching of alkanes
3	1649	1612	−12	N–H bend of alkenes
4	1423	1462	39	C–C (in ring) stretching of aromatics
5	1254	1254	0	C–N stretching of aromatic amines
6	1115	1094	−21	C–N stretching of aliphatic amines
7	910	920	10	O–H bending of carboxylic acids
8	635	773	38	C–Cl stretch of alkyl halides

The EDX spectra (Figure 4) and data of the adsorbent are shown in Table 2. From Table 2, it can be deduced that activation of the adsorbent increased the carbon content of MOSPAC. Since adsorption capacity is a function of the active carbon present in a sample, this implies that acid activation has led to increased adsorption capacity of the adsorbent [48,49].

Oxygen containing functional groups (Boehm titration)

Boehm's technique was used to characterize the surface chemical property of the adsorbent. Several assumption were made before the surface acidity and basicity could however be calculated. It was assumed that acidic group generally, could only be neutralized by NaOH, Na_2CO_3 and $NaHCO_3$ while all basic groups would be neutralized by HCl. Table 3 shows the summary of the properties of the surface functional groups through the Boehm titration. The total acidic group for the activated carbon produced from moringa seed pod is 1.038 mmol/g, while the total basic group value is 0.054 mmol/g, this shows that the basic group is lower when compared with the acidic group. The significant increase of acidic groups when compared to the basic group, suggests that the majority of functional group on the adsorbent surface are acidic. Prominent acidic group indicate more oxygenated functional groups, resulting in higher adsorption of dyes [50,51].

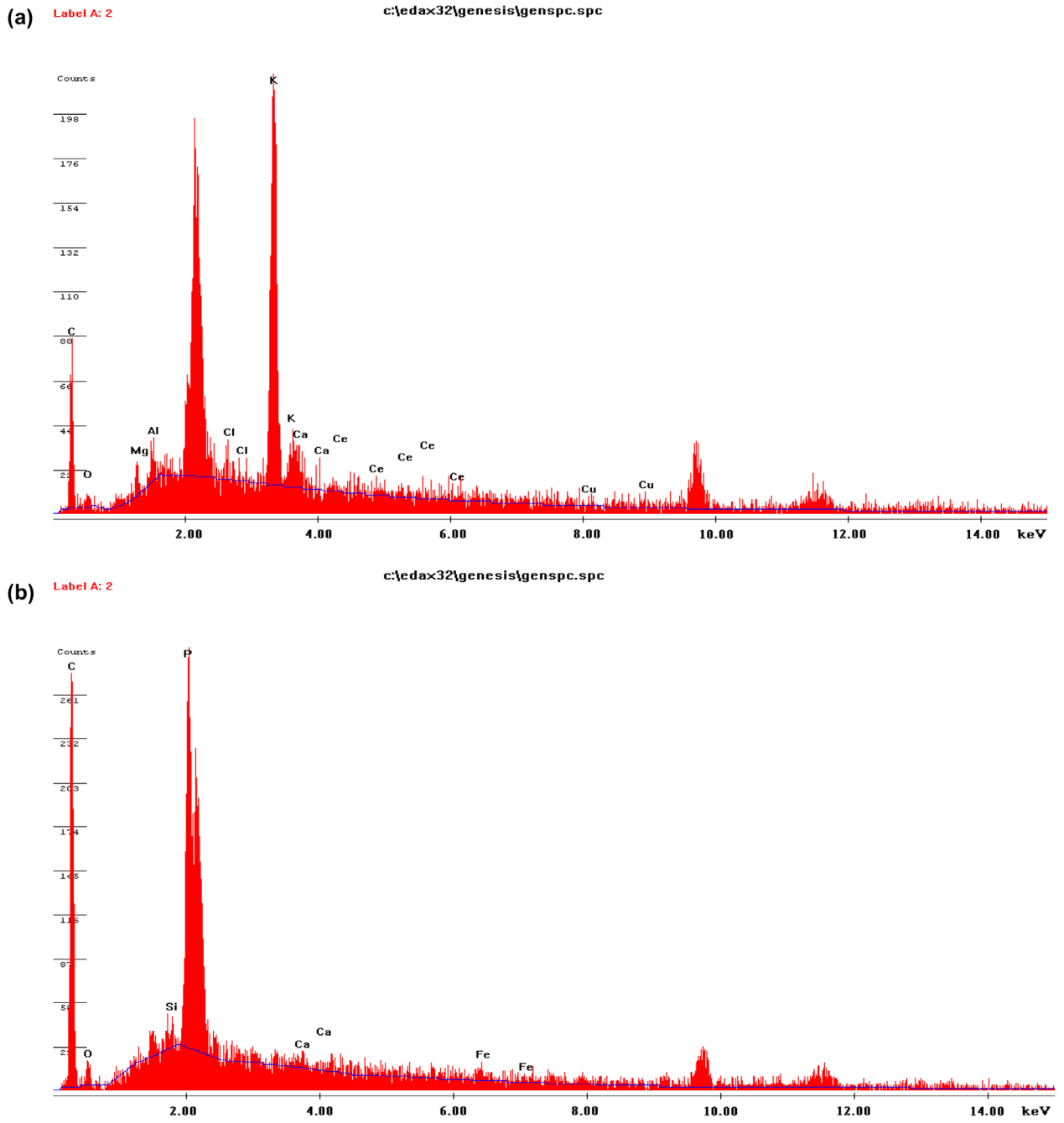

Figure 4. EDX spectra of (a) MOSPR (b) MOSPAC.

Table 2a. Energy dispersive X-ray (EDAX ZAF) quantification of MOSPR.

Element	Wt. %	At %	*K*-ratio	*Z*	*A*	*F*
C	61.69	81.18	0.2522	1.0356	0.3947	1.0001
O	6.28	6.20	0.0083	1.0183	0.1304	1.0001
Me	2.13	1.38	0.0115	0.9772	0.5531	1.0017
Al	1.97	1.15	0.0125	0.9485	0.6686	1.0024
Cl	2.15	0.96	0.0195	0.9181	0.9636	1.0235
K	13.92	5.63	0.1299	0.9251	0.9952	1.0140
Ca	6.08	2.40	0.0542	0.9470	0.9388	1.0030
Ce	2.55	0.29	0.0199	0.7319	1.0616	1.0027
Cu	3.24	0.80	0.0269	0.8307	1.0016	1.0000
Total	100.00	100.00				

Table 2b. Energy dispersive X-ray (EDAX ZAF) quantification of MOSPAC.

Element	Wt. %	At %	*K*-ratio	*Z*	*A*	*F*
C	78.44	88.80	0.2367	1.0156	0.2971	1.0001
O	5.23	4.44	0.0076	0.9987	0.1451	1.0002
Si	1.32	0.64	0.0117	0.9579	0.9124	1.0028
P	12.20	5.36	0.1074	0.9193	0.9573	1.0004
Ca	0.74	0.25	0.0069	0.9273	1.0014	1.0020
Fe	2.07	0.50	0.0177	0.8410	1.0180	1.0000
Total	100.00	100.00				

Table 3. Different functional groups on MOSPAC.

	Different functional groups on MOSPAC				
Adsorbent	Carboxylic (mmolg^{-1})	Phenolic (mmolg^{-1})	Lactonic (mmolg^{-1})	Basic (mmolg^{-1})	Acidic (mmolg^{-1})
MOSPAC	0.696	–	0.341	0.054	1.037

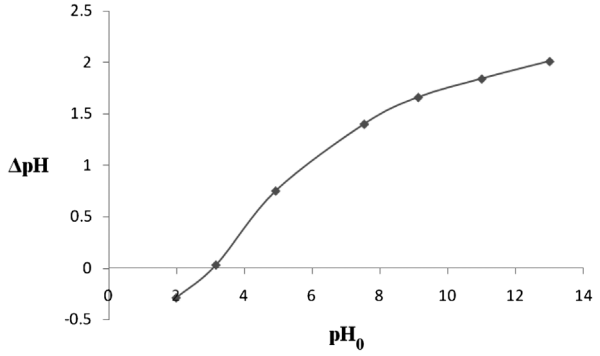

Figure 5. Plot of pH_{pzc} of acid activated *moringa oleifera* seed pod (MOSPAC).

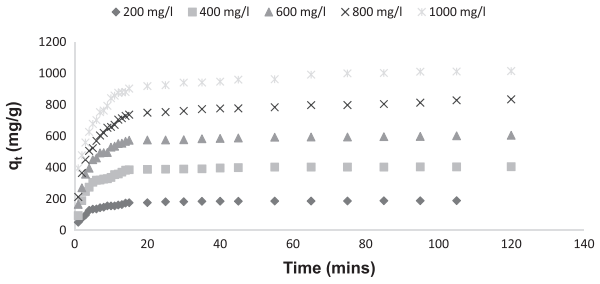

Figure 6. Plot of adsorption of Rh-B dye onto MOSPAC against adsorption time at various initial dye concentrations at 30 °C.

pH point of zero charge (pH_{PZC})

The pH point of zero charge of MOSPAC was determined, the results is as shown in Figure 5. The value was determined where the resulting curve cut through the pH_0 axis as shown in Figure 5. The pH_{PZC} was found to be 3.05 for MOSPAC. Cation adsorption is enhanced at pH value higher than pH_{PZC}, while adsorption of anions is favoured at pH value less than pH_{PZC} [41,50–52].

Batch adsorption studies

The effect of contact time and initial Rh-B dye concentration

The effect of contact time on adsorption of Rh-B dye onto MOSPAC at various initial concentrations (200–1000 mg/L) at 30 °C is presented in Figure 6. The adsorption rate increased with time at the initial stage and became slower before reaching equilibrium. This can be attributed to the fact that vacant sites were available on the adsorbents at the initial stage. This developed a strong driving force for dye molecules to overcome the mass transfer resistance between aqueous and solid phases. After a period of time, the remaining surface site became difficult to occupy due to the electrostatic

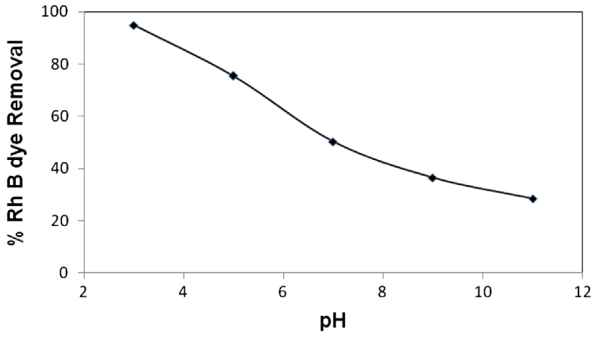

Figure 7. Plot of percentage Rh-B dye removal at different pH.

hindrance or repulsive forces that exist between the dye molecules and the surface of adsorbent. At this point, equilibrium was reached. This stage also reflects the maximum adsorption capacity of each adsorbent under certain operating conditions [42]. Apart from this, the time required for adsorption process to reach equilibrium stage is strongly dependent on the initial dye concentration. At higher initial dye concentration, the amount of dye adsorbed at equilibrium was high. For Rh-B dye adsorption onto MOSPAC, at 200 mg/L initial concentration, the maximum adsorption uptake was 188.93 mg/g while that at 1000 mg/L was 1014.99 mg/g. At higher initial concentration, the concentration gradient was higher, thereby developing a higher driving force during the adsorption process. As a result of the increased diffusion process, the equilibrium adsorption uptake increased [53]. When the initial concentration was low, the ratio of dye molecules to vacant sites was smaller, and this indirectly led to higher amount of dye removal in solution.[54] As the initial concentration increased, the ratio of dye molecules to vacant sites increased and most of the vacant sites become saturated. At this stage, dye molecules tend to compete among themselves to diffuse into the internal pores, resulting in lower percentage dye removal. [54].

Effect of adsorbent dosage

The amount of RhB dye adsorbed decreased with increase in adsorbent dosage. Maximum sorption was obtained at 0.1 g of adsorbent dosage (Figure not shown). As expected, percentage Rh-B dye removal increased with the increasing amount of adsorbent; however, the amount of dye adsorbed unto MOSPAC (mg/g) decreased with increasing amount of adsorbent. When the adsorbent dose was increased from 0.1 to 0.5 g, the amount of Rh-B dye adsorbed decreased from 96.43 to 31.62 mg/g. This can be attributed to overlapping or aggregation of adsorption sites, resulting in a decrease

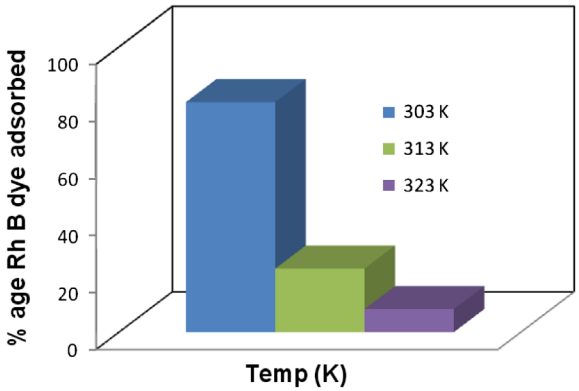

Figure 8. Plot of percentage Rh-B dye removal at different temperatures.

in total adsorbent surface area available to the dye and an increase in path length [55]. The same behavior has been reported by other authors [56]. As a result of this, 0.1 g of MOSPAC was chosen for subsequent studies.

Effect of pH on dye adsorption

The effect of pH on the adsorption of RhB dye onto MOSPAC was studied. The result is as shown in Figure 7. The uptake of RhB at pH 3.01 was 94.76%, at pH 9.0, it was observed that the uptake decreases with increase in pH (36.45%) (Figure 7). The change in pH of the solution results in the formation of different ionic species and surface charge. At pH values lower than pH_{pzc} (3.05), the RhB dye are of cationic and monomeric molecular forms [57], thus the dye molecule can enter easily into the pore structure of the adsorbent. At pH value higher than pH_{pzc}, the zwitterionic forms of RhB dye exist in solution mixture. This form increases the aggregation of RhB dye molecule to form larger molecules (dimers). These molecules are unable to enter the pores as a result of their size thereby resulting in lower percentage removal at high pH (36.45%). Ghanadzadeh et al., [58] also studied the aggregation of RhB dye in the microporous solid hosts. Lopez Arbeloa and Ruiz Ojeda [59] determined the equilibrium constant for the dimer – momoner transition of RhB dye in aqueous solution. The greater aggregation of the zwitterionic form is due to the attractive electrostatic interactions between the carboxyl and xanthenes groups of the monomers [60].

Effect of temperature on adsorption of Rh-B dye

Temperature is an important parameter that influence dye adsorption. The effect of RhB dye adsorption onto MOSPAC as a function of temperature is shown in Figure 8. It is clear that adsorption of dye decreased when the temperature was increased, which reveal the exothermic adsorption process of Rh-B dye onto MOSPAC. The maximum amount of dye adsorbed was 80.64% (1250 mg/g) at 303 K, while 8.06% (125 mg/g) was adsorbed at 323 K respectively. Percentage removal showed that increase in temperature leads to reduction in percentage of dye removed (Figure 8). The decrease in dye adsorption at higher temperature was due to the weakening of supportive forces between active sites on the adsorbent and dye to that between adjacent dye molecules during adsorption process [61]. A sharp reduction after 303 K was due to the decrease in surface activity at higher temperature, which indicates that the adsorption process was exothermic and Rh-B dye adsorption onto MOSPAC occured mainly by physical adsorption [62]. In other reported studies, palm kernel fibre gave similar adsorption pattern for anionic dyes as a function of temperature [63]. Therefore, Rh-B dye molecule desorbed at higher temperature was due to deterioration of adsorptive forces between dye molecule and functional groups on the adsorbent surface.

Adsorption isotherms

Table 4a reports the parameters of the isotherm models employed in this study at 30 °C. These models are: Langmuir, Freundlich, Temkin, and Dubinin-Radushkevich. The suitability of these models were determined by choosing the model with the value of R^2 closest to 1. According to theoretical Langmuir adsorption isotherm, it assumes that the maximum monolayer adsorption occurs when the surface is covered by a monolayer of adsorbate. This isotherm can be used to determine the highest adsorption capacity that corresponds

Table 4a. Isotherm parameters for Rh-B dye adsorption onto MOSPAC at 30 °C.

Langmuir		Freundlich		Temkin		DBR	
q_m (mg/g)	1250	K_f	139.4	K_T (mol/g)	8.592	X_m (mg/g)	934.4
K_L (l/mg)	0.1096	n	1.817	b_T (mol/kJ)	0.0142	β (10^{-6})	1.00
R_L	0.0086	$1/n$	0.5504	R^2	0.9940	E_a (kJ/mol)	0.707
R^2	0.9979	R^2	0.9920			R^2	0.9968

Table 4b. Isotherm parameter for Rh-B dye adsorption onto MOSPAC at 40 °C.

Langmuir		Freundlich		Temkin		DBR	
q_m (mg/g)	175.4	K_f	629.7	K_T (mol/g)	15.61	X_m (mg/g)	181.6
K_L (l/mg)	2.5915	n	1.542	b_T (mol/kJ)	0.0120	β (10^{-6})	1.00
R_L	0.0004	$1/n$	0.6486	R^2	0.9080	E_a (kJ/mol)	2.236
R^2	1.0000	R^2	0.9893			R^2	0.9989

Table 4c. Isotherm parameters for Rh-B dye adsorption onto MOSPAC at 50 °C.

Langmuir		Freundlich		Temkin		DBR	
q_m (mg/g)	125	K_f	81.4	K_T (mol/g)	3.626	X_m (mg/g)	944.0
K_L (l/mg)	0.1538	n	1.304	b_T (mol/kJ)	0.0054	β (10^{-6})	−9
R_L	0.0060	$1/n$	0.767	R^2	0.9974	E_a (kJ/mol)	0.2357
R^2	0.9981	R^2	0.9224			R^2	0.9976

Table 5. Comparison of maximum monolayer adsorption capacities of Rh-B dye on various adsorbents.

Adsorbents	q_m (mg/g)	References
Modified Coir pith	14.90	[64]
Baker's yeast	25.00	[65]
Cedar cone	4.55	[66]
Sugarcane baggase	51.50	[67]
Acid treated Kaolinite	23.70	[68]
Acid treated montmorillonite	188.67	[68]
Raw dika nut waste	212.77	[69]
Acid treated dika nut waste	232.00	[69]
Raphia hookerie fruit epicarp	666.67	[56]
Jute stick powder	87.70	[70]
Microwave treated nilotica leaf	24.39	[71]
Fly ash	10.00	[72]
Artocarpus odoratissimus	131.00	[46]
Casuarina equisetifolia cone powder	49.50	[47]
Peat from Brunei Darussalam	162.90	[73]
Moringa olifera seed pod	*1250.00*	*This work*

to the complete monolayer coverage on MOSPAC. The values of q_m at different temperatures are shown in Tables 5. Maximum q_m was 1250.0 mg/g at 30 °C. Comparison of the maximum monolayer adsorption capacities of Rh-B dye onto various adsorbents revealed that MOSPAC is an effective adsorbent (Table 5). The Freundlich isotherm is used to illustrate the non-ideal heterogeneous behavior of the adsorption process. The extent of adsorption can be reflected by the value of K_f. It was found that the extent of adsorption at 50 °C (K_f = 81.4) was approximately 1.71 times lesser than that of 30 °C (K_f = 139.4). The value of $1/n$ calculated from the Freundlich model was lesser than 1. The equilibrium binding constant, b_T (mol/g) which is the Temkin isotherm constant, was determined from the Temkin isotherm model. The Dubinin-Radushkevich isotherm model can be used to examine the porosity apparent free energy, E and the characteristics of the adsorption process. The values of E_a for MOSPAC at 30, 40, and 50 °C are 0.707, 2.236, and 0.236 kJ/mol respectively. Since all these values range between 1 and 8 kJ/mol, it shows that physisorption was responsible for the adsorption of Rh-B dye onto MOSPAC [35,36]. After summarizing all the important parameters for each isotherm, the value of R^2 was used to judge the most suitable model for the adsorption of Rh-B dye onto MOSPAC. The results obtained were: Freundlich (R^2 = 0.992) < Temkin (R^2 = 0.994) < Dubinin-Radushkevich (R^2 = 0.996) < Langmuir (R^2 = 0.998). Error analysis was conducted in other to identify the model that fitted most. The standard errors of the mean for the entire isotherm studied were carried out. Langmuir (±0.00069), Freundlich (±0.022783), Temkin (±0.029427) and D-R (±0.0353). The isotherm with the least error was Langmuir. The isotherm with the highest R^2 value and the least error was Langmuir. These findings suggests that the adsorption process can best be described using the Langmuir model. The Langmuir equation can be expressed in a term of dimensionless separation factor, R_L. The value of R_L reflects the type of isotherm to be either: (i) irreversible (R_L = 0); (ii) favorable (0 < R_L < 1); (iii) linear (R_L = 1); or (iv) unfavorable (R_L < 1). From Table 4a–c, it was obvious that the value of R_L was in the range of 0–1 for the adsorption process. This indicates that the adsorption of Rh-B dye onto MOSPAC was favorable [74].

Adsorption kinetic studies

In order to investigate the adsorption kinetics of Rh-B dye, four different kinetic models, namely pseudo-first-order, pseudo-second-order, Elovich and intraparticle diffusion models were used in this study. The pseudo-first-order kinetic model was use to predict the adsorption kinetics. Plots of ln ($q_e - q_t$) vs. t gave a straight line, with negative slope of k_1 and intercept of ln q_e. Inferring from the values of R^2 obtained from the adsorption of Rh-B dye onto MOSPAC, R^2 values are lower than those obtained for the pseudo-second-order model. On the other hand, the plots of t/q_t vs. t for the pseudo-second-order model were also used to study the adsorption process. As can be seen from Table 6, the values of R^2 calculated for the adsorption process are higher than that obtained for the pseudo-first order model. This shows that adsorption of Rh-B dye onto MOSPAC fitted the pseudo-second order model. Similarly, the Elovich model was used to describe the pseudo second-order kinetics by assuming that the actual solid surfaces are energetically heterogeneous. Theoretically, when there is increase in solution temperature, the extent of surface coverage, b should decrease owning to the fact that the number of sites available for trapping the dye molecules will be less at higher temperature. Unfortunately, the low values of R^2, ranging from 0.78 to 0.9019 in the adsorption process shows that the experimental data did not agree with the Elovich kinetic model [75]. Comparing the values of R^2 for the kinetic equations used, adsorption of Rh-B dye onto MOSPAC can be described by the following kinetic order: pseudo-second-order > pseudo-first-order > Elovich. Adsorption rate is controlled by several factors which include: diffusion of the solute from the solution to the film surrounding the particle, diffusion from the medium to the particle surface, diffusion from the surface to the internal sites (surface diffusion or pore diffusion) and uptake which can involve several

Table 6. Parameters of the pseudo-first order, pseudo-second order and Elovich kinetic models together with their regression coefficient for MOSPAC at 30 °C.

	200 mg/l	400 mg/l	600 mg/l	800 mg/l	1000 mg/l
Pseudo-first order kinetic model					
k_1 (min^{-1})	0.0550	0.0528	0.0385	0.0325	0.0443
$q_{e\,calc}$ (mg/g)	62.565	108.245	144.301	284.975	370.591
$q_{e\,exp}$ (mg/g)	188.933	406.089	605.522	834.444	1014.989
SSE (%)	24.320	56.287	87.163	103.840	121.780
R^2	0.8937	0.8746	0.7885	0.8395	0.9318
Pseudo-second order kinetic model					
k_2 (min^{-1})	0.0023	0.0013	0.0009	0.0004	0.0004
$q_{e\,calc}$ (mg/g)	192.308	416.667	625.000	833.333	1000.000
$q_{e\,exp}$ (mg/g)	188.933	406.089	605.522	834.444	1014.989
SSE (%)	0.650	1.999	3.681	0.210	2.833
h	85.059	225.695	351.563	277.778	400.000
R^2	0.9998	0.9998	0.9999	0.9995	0.9998
Elovich model					
B	0.0374	0.0194	0.0134	0.0090	0.0080
α	627.831	2652.872	4644.563	2865.565	6148.686
R^2	0.8495	0.7902	0.7800	0.8762	0.9019

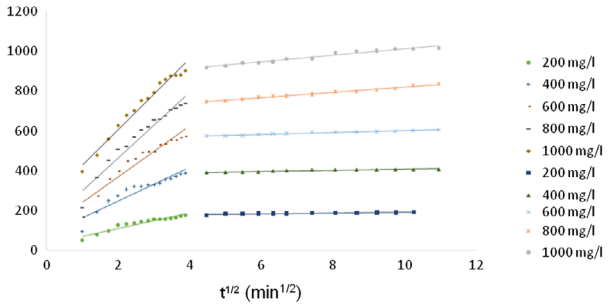

Figure 9. Plot of intraparticle diffusion model for Rh-B dye adsorption onto MOSPAC.

mechanisms such as physicochemical adsorption, ion-exchange, precipitation or complexation [76,77]. The most important mechanism controlling adsorption kinetics is the diffusion mechanisms such as the initial curved portion which occurred due to rapid external diffusion and surface adsorption [78]. In this study, the plots obtained were multi linear. The first and sharper portion is attributed to the boundary layer diffusion of CR dye molecules, whereas the second portion corresponds to the gradual adsorption stage, where intraparticle diffusion was the rate-limiting step. Mass transfer is governed by several relationships, taking into account the diffusion mechanisms and their related equations, the coupling between liquid and solid phases and the initial and boundary conditions. Therefore, it means that the rate of equilibrium attainment may be intraparticle-diffusion controlled [79]. Following the fast phase, there was a gradual adsorption stage, where intraparticle diffusion is rate controlling. Thereafter, adsorption became very slow and stable, approaching an equilibrium stage and maximum adsorption, i.e. a plateau profile. Similar findings were reported by Vimonses and coworkers [80]. The plot of q_t vs. $t^{1/2}$ profiles of Rh-B dye adsorption by MOSPAC adsorbents was non-linear (Figure 9). The deviation from the origin shows that intraparticle transport is not the only rate-limiting step. It can be seen, however, that the second adsorption stage is characterized by the intra-particle diffusion. This is the rate-controlling step for the adsorption process of the modified MOSPAC. The plots did not pass through the origin (i.e. $C \neq 0$). This shows that the intra-particle diffusion occurred in the adsorption process, but was not the only parameter controlling the rate of the reaction. The intercepts C, are proportional to the boundary layer thickness. The extent of thickness of boundary layer was observed from the MOSPAC at 30 °C. The effect of boundary layer increases with the value of C [81,82]. The boundary layer also helps to know the tendency of the adsorbent to adsorb the dye or remain in solution. Higher values of C, i.e. the boundary layer thickness, depict higher adsorption capacities (Table 7).

Adsorption thermodynamics

Thermodynamic parameters are important in adsorption studies; they provide a better understanding of the effect of temperature on the adsorption process. The thermodynamic parameters are tabulated in Table 8. The positive values of ΔH° obtained in the adsorption of RhB dye onto MOSPAC signify that the adsorption process was endothermic in nature (Table 8). The ΔH° value was calculated to be 127.56 kJ/mol. The positive values of ΔS° indicate that increase in randomness occurred at solid-solution interface during the adsorption process. This indirectly shows the affinity of adsorbent toward dye molecules [74]. As contained in Table 8, ΔG° values were negative at all temperatures studied, inferring that the adsorption was spontaneous in nature. Since the values of ΔG° decreased with increasing temperature, it suggests that at higher temperature, the driving force was less, resulting in lower adsorption uptake [83]. The values of E_a obtained fall within the energy range of 0–40 kJ/mol, it connotes that the adsorption process was physisorption.

Table 7. Parameters of the intra-particle kinetic model together with their regression coefficients for MOSPAC at 30 °C.

	200 mg/l	400 mg/l	600 mg/l	800 mg/l	1000 mg/l
k_{diff1}	38.960	84.367	128.020	164.700	177.470
C_1	31.970	79.362	114.760	136.940	253.780
R^2_1	0.9181	0.8833	0.9190	0.9486	0.9763
k_{diff2}	1.6707	2.8442	4.6599	12.8430	16.3400
C_2	172.800	377.850	554.810	691.100	841.920
R^2_2	0.8062	0.8422	0.9590	0.9839	0.9629

Table 8. Thermodynamic parameters for adsorption of Rh-B dye onto MOSPAC.

Temp (K)	ΔG° (kJ mol^{-1})	ΔH° (kJ mol^{-1})	ΔS° (Jk^{-1} mol^{-1})	E_a (kJ mol^{-1})	A (10^{11})
303	−27.381	127.562	507.894	33.780	2.023
313	−36.515				
323	−30.096				

Conclusions

In this study, the potential of MOSPAC for the adsorption of Rh-B dye was investigated. Findings revealed that *moringa oleifera* seed pod wastes are useful precursors in the preparation of alternative adsorbents in lieu of expensive commercial activated carbon. Optimum Rh-B dye adsorption was observed at pH 3.01. Characterization revealed that MOSPAC has large pores resulting in high dye adsorption activity. Adsorption data was best fitted using Langmuir Isotherm and pseudo-second-order kinetic model. The study shows that *moringa oleifera* seed pod was both effective as well as economically viable adsorbent for Rh-B dye removal from wastewaters.

Acknowledgments

The corresponding author acknowledges the support obtained from The World Academy of Science (TWAS) in form of grants; Research grant number: 11–249 RG/CHE/AF/AC_1_UNESCO FR: 3240262674 (2012) and 15–181 RG/CHE/AF/AC_1_: 3240287083 (2015) respectively.

Disclosure statement

No potential conflict of interest was reported by the authors.

Funding

This work was supported by The World Academy of Science (TWAS) in form of grants; Research [grant number 11–249 RG/CHE/AF/AC_1_UNESCO FR: 3240262674 (2012)], [grant number 15–181 RG/CHE/AF/AC_1_: 3240287083 (2015)].

References

[1] Wang L, Zhang J, Zhao R, et al. Adsorption of basic dyes on activated carbon prepared from Polygonum orientale Linn: equilibrium, kinetic and thermodynamic studies. Desalination. 2010;254:68–74.

[2] Sivaraj R, Namasivayam C, Kadirvelu K. Orange peel as an adsorbent in the removal of acid violet 17 (acid dye) from aqueous solutions. Waste Manag. 2001;21:105–110.

[3] De Lima ROA, Bazo AP, Salvadori DMF, et al. Mutagenic and Carcinogenic potential of a textile azo dye processing plant effluent that impacts a drinking water source. Mutat Res. 2007;626(1–2):53–60.

[4] Somasekhara Reddy MC, Sivaramakrishna L, Varada Reddy A. The use of an agricultural waste material, Jujuba seeds for the removal of anionic dye (Congo red) from aqueous medium. J Hazard Mater. 2012;203–204:118–127.

[5] Meric S, Selcuk H, Belgiorno V. Acute toxicity removal in textile finishing wastewater by Fenton's oxidation, ozone and coagulation–flocculation processes. Water Res. 2005;39:1147–1153.

[6] Phalakornkule C, Polgumhang S, Tongdaung W, et al. Electrocoagulation of blue reactive, red disperse and mixed dyes, and application in treating textile effluent. J Environ Manag. 2010;91:918–926.

[7] Paschoal FMM, Anderson MA, Zanoni MVB. The photoelectrocatalytic oxidative treatment of textile wastewater containing disperse dyes. Desalination. 2009;249:1350–1355.

[8] Gupta N, Kushwaha AK, Chattopadhyaya MC. Application of potato (*Solanum tuberosum*) plant wastes for the removal of methylene blue and malachite green dye from aqueous solution. Arab J Chem. 2016;9:S707–S716. DOI: 10.1016/j.arabjc.2011.07.021.

[9] Dhale AD, Mahajani VV. Studies in treatment of disperse dye waste: membrane-wet oxidation process. Waste Manag. 2000;20(1):85–92.

[10] Kim HG, Park C, Yang J, et al. Optimization of back flushing conditions for ceramic ultrafiltration membrane of disperse dye solutions. Desalination. 2007;202:150–155.

[11] Gerçel O, Gerçel HF, Koparal AS, et al. Removal of disperse dye from aqueous solution by novel adsorbent prepared from biomass plant material. J Hazard Mater. 2008;160:668–674.

[12] Srinivasan A, Viraraghavan T. Decolorization of dye wastewaters by biosorbents: a review. J Environ Manag. 2010;91:1915–1929.

[13] Gaikwad RW, Misal SA. Sorption studies of methylene blue on silica gel. Int J Chem Eng Appl. 2010;4:342–345.

[14] Ho YS, Chiang CC. Sorption studies of acid dye by mixed sorbents. Adsorption. 2001;7:139–147.

[15] Ahmad MA, Ahmad N, Bello OS. Adsorptive removal of malachite green dye using durian seed-based activated carbon. Water Air Soil Pollut. 2014;225:2057. DOI: 10.1007/s11270-014-2057-z.

[16] Ahmad MA, Ahmad N, Bello OS. Modified durian seed as adsorbent for the removal of methyl red dye from aqueous solutions. Appl Water Sci. 2015;5:407–423. DOI: 10.1007/s13201-014-0208-4.

[17] Bello OS, Bello OU, Ibrahim OL. Adsorption characteristics of mango leaf (*Mangifera indica*) powder as adsorbent for Malachite green dye removal from aqueous solution. Cov J Phys Life Sci. 2014;2:1–13.

[18] Gupta VK, Jain R, Varshney S. Removal of reactofix golden yellow 3 RFN from aqueous solution using wheat husk – an agricultural waste. J Hazard Mater. 2007;142:443–448.

[19] Bello OS, Ahmad MA. Coconut (Cocos nucifera) shell based activated carbon for the removal of malachite green dye from aqueous solutions. Sep Sci Technol. 2012;47:903–912.
[20] Bello OS, Adeogun IA, Ajaelu JC, et al. Adsorption of methylene blue onto activated carbon derived from periwinkle shells: kinetics and equilibrium studies. Chem Ecol. 2008;24:285–295.
[21] Gupta VK, Mittal A, Krishnan L, et al. Adsorption treatment and recovery of the hazardous dye, Brilliant Blue FCF, over bottom ash and de-oiled soya. J Colloid Interface Sci. 2006;293:16–26.
[22] Gupta VK, Suhas S. Application of low-cost adsorbents for dye removal – a review. J Environ Manage. 2009;90(8):2313–2342.
[23] Mittal A, Gupta VK, Malviya A, et al. Process development for the batch and bulk removal and recovery of a hazardous, water soluble azo dye Metanil Yellow by adsorption over waste materials (bottom ash and de-oiled Soya). J Hazard Mater. 2008;151:821–832.
[24] Khan TA, Khan EA. Adsorptive uptake of basic dyes from aqueous solution by novel brown linseed deoiled cake activated carbon: equilibrium isotherms and dynamics. J Environ Chem Eng. 2016;4(3):3084–3095.
[25] Khan TA, Rahman R, Khan EA. Adsorption of malachite green and methyl orange onto waste tyre activated carbon using batch and fixed-bed techniques: isotherm and kinetics modeling. Model Earth Syst Environ. 2017;3:38. DOI: 10.1007/s40808-017-0284.
[26] Ali I, Dahiya S, Tabrez K. Removal of direct red 81 dye from aqueous solution by native and citric acid modified bamboo sawdust-Kinetic study and equilibrium isotherm analyses. Gazi Univ J Sci. 2012;25:59–87.
[27] Khan TA, Sharma S, Khan EA, et al. Removal of congo red and basic violet 1 by chir pine (Pinus roxburghii) sawdust, a saw mill waste: batch and column studies. Toxicol Environ Chem. 2014;96:555–568.
[28] Khan TA, Nazir M. Enhanced adsorptive removal of a model acid dye bromothymol blue from aqueous solution using magnetic chitosan-bamboo sawdust composite: batch and column studies. Environ Prog Sustain Energy. 2015;34:1444–1454.
[29] Khan TA, Nazir M, Khan EA, et al. Multiwalled carbon nanotube–polyurethane (MWCNT/PU) composite adsorbent for safranin T and Pb (II) removal from aqueous solution: batch and fixed-bed studies. J Mol Liq. 2015;212:467–479.
[30] Khan TA, Nazir M, Khan EA. Magnetically modified multiwalled carbon nanotubes for the adsorption of bismarck brown R and Cd (II) from aqueous solution: batch and column studies. Desalin Water Treat. 2016;57:19374–19390.
[31] Khan TA, Dahiya S, Khan EA. Removal of direct red 81 from aqueous solution by adsorption onto magnesium oxide-coated kaolinite: isotherm, dynamics and thermodynamic studies. Environ Prog Sustain Energy. 2017;36:45–58.
[32] Langmuir I. Adsorption of gases on plane surfaces of glass, mica and platinum. J Am Chem Soc. 1918;40:1361–1403.
[33] Freundlich HMF. Over the adsorption in solution. J Phys Chem. 1906;57:385–470.
[34] Temkin MJ, Pyzhev V. Recent modifications to Langmuir isotherms. Acta Physiochim USSR. 1940;12:217–222.
[35] Dubinin MM. The potential theory of adsorption of gases and vapors for adsorbents with energetically non-nniform surface chemistry. Chem Rev. 1960;60:235–241.
[36] Ajemba RO. Adsorption of malachite green from aqueous solution using activated ntezi clay: optimization, isotherm and kinetic studies. Int J Eng Trans C Asp. 2014;27(6):839–854.
[37] Lagergren S. Zurtheorieder sogenannten adsorption gelosterstoffe [On the theory of so-called adsorption of materials]. kungliga Svenska Veteriskaps akademiens. Handlingar. 1898;24:1–39.
[38] Ho YS, Mckay G. The kinetics of sorption of basic dyes from aqueous solution by sphagnum moss peat. Can J Chem Eng. 1998;76(4):822–827.
[39] Aharoni C, Ungarish M. Kinetics of activated chemisorptions. Part I: the non-Elovichian part of the isotherm. J Chem Soc Farad Trans. 1976;72:265–268.
[40] Weber WJ, Morris JC. Kinetics of adsorption on carbon from solution. J Sanitary Eng Div ASCE. 1962;89:31–59.
[41] Almeida CAP, Debacher NA, Downs AJ, et al. Removal of methylene blue from coloured effluents by adsorption on montmorillonite clay. J Colloid Interface Sci. 2009;332:46–53.
[42] Bhadusha N, Ananthabaskaran T. Adsorptive removal of methylene blue onto $ZnCl_2$ activated carbon from wood apple outer shell: kinetics and equilibrium studies. J Chem. 2011;8:1696–1707.
[43] Boehm HP. Surface oxides on carbon and their analysis: a critical assessment. Carbon. 2002;40:145–149.
[44] Hameed BH, Ahmad AA. Batch adsorption of methylene blue from aqueous solution by garlic peel, an agricultural waste biomass. J Hazard Mater. 2009;164:870–875.
[45] Auta M, Hameed BH. Optimized waste tea activated carbon for adsorption of methylene blue and acid blue 29 dyes using response surface methodology. Chem Eng J. 2011;175:233–243.
[46] Lim LBL, Priyantha N, Fang XY, et al. Artocarpus odoratissimus peel as a potential adsorbent in environmental remediation to remove toxic Rhodamine B dye. J Mater Environ Sci. 2017;8(2):494–502.
[47] Dahri MK, Kooh MRR, Lim LBL. Remediation of Rhodamine B dye from aqueous solution using Casuarina equisetifolia cone powder as a low cost adsorbent. Adv Phys Chem. 2016;2016:7. Article ID 9497378.
[48] Okeola, OF. Preparation and characterization of activated carbon from various waste materials [M. Sc. Thesis]. University of Ilorin; 1999;5:18–37.
[49] Dada AO, Inyinbor AA, Oluyori AP. Comparative adsorption of dyes unto activated carbon prepared from maize stems and sugar cane stems. J Appl Chem. 2012;2:38–43.
[50] Farahani M, Abdullah S, Hosseini S, et al. Adsorption-based cationic dyes using the carbon active sugarcane bagasse. Proc Environ Sci. 2011;10:203–208.
[51] Bello OS, Owojuyigbe ES, Babatunde MA, et al. Sustainable conversion of agro-wastes into useful adsorbents. Appl Water Sci. 2016 (In press). DOI:10.1007/s13201-016-0494-0.
[52] Hamadaoui O. Removal of Rhodamine B from aqueous solutions by tea waste. J Hazard Mater. 2006;135:264–273.
[53] Baek MH, Ijagbemi CO, Se-Jin O, et al. Removal of Malachite Green from aqueous solution using degreased coffee bean. J Hazard Mater. 2010;176:820–828.
[54] Al-Degs Y, Khraisheh MAM, Allen SJ, et al. Effect of carbon surface chemistry on the removal of reactive dyes from textile effluents. Water Res. 2000;34:927–935.
[55] Garg VK, Kumar R, Gupta R. Removal of malachite green dye from aqueous solution by adsorption using agro-industry waste: a case study of prosopis cineraria. Dyes Pigm. 2004;62:1–10.
[56] Iyinbor AA, Adekola FA, Olatunji GA. Kinetics, isotherm and thermodynamic modelling of liquid phase adsorption of Rhodamine B dye onto Raphia hookerie fruit epicarp. Water Res Ind. 2016;15:14–27.

[57] Deshpande AV, Kumar U. Effect of method of preparation on photophysical properties of Rh B impregnated sol-gel hosts. J Non-Cryst Solids. 2002;306(2):149–159.
[58] Ghanadzadeh A, Zanjanch MA, Tribandpay R. The role of host environment on the aggregative properties of some ionic dye materials. J Mol Struct. 2002;616:167–174.
[59] López Arbeloa I, Ruiz Ojeda P. Dimeric states of Rhodamine B. Chem Phys Lett. 1982;87(6):556–560.
[60] Lin C, James AR, Branko NP. Correlation of double-layer capacitance with the pore structure of sol-gel derived carbon xerogels. J Electrochem Soc. 1999;146(10):3639–3643.
[61] Ho YS, Chiu WT, Wang CC. Regression analysis for the sorption isotherms of basic dyes on sugarcane dust. Bioresour Technol. 2005;96:1285–1291.
[62] Aksu Z, Tezer S. Biosorption of reactive dyes on the green alga Chlorella vulgaris. Process Biochem. 2005;40: 1347–1361.
[63] Ofomaja AE, Ho YS. Equilibrium sorption of anionic dye from aqueous solution by palm kernel fibre as sorbent. Dyes Pigm. 2007;74:60–66.
[64] Sureshkumar MV, Namasivayam C. Adsorption behavior of direct red 12B and Rhodamine B from water unto surfactant modified coconut coir pith. Colloids Surf A Physicochem Eng Asp. 2008;317(1–3):277–283.
[65] Yu J, Li B, Sun X, et al. Adsorption of methylene blue and rhodamine B on baker's yeast and photocatalytic regeneration of the biosorbent. Biochem Eng J. 2009;45:145–151.
[66] Zamouche M, Hamdaoui O. Sorption of Rhodamine B by cedar cone: effect of pH and ionic strength. Energy Procedia. 2012;18:1228–1239.
[67] Zhang Z, O'Hara IM, Kent GA, et al. Comparative study on adsorption of two cationic dyes by milled sugarcane bagasse. Ind Crops Prod. 2013;42:41–49.
[68] Bhattacharyya KG, SenGupta S, Sarma GK. Interactions of the dye, Rhodamine B with kaolinite and montmorillonite in water. Appl Clay Sci. 2014;99:7–17.
[69] Iyinbor AA, Adekola FA, Olatunji GA. Adsorption of Rhodamine B dye from aqueous solution on Irvingin gabonesis Biomass: kinetics and thermodynamic studies. S Afr J Chem. 2015;68:115–125.
[70] Panda GC, Das SK, Guha AK. Jute stick powder as a potential biomass for the removal of Congo red and Rhodamine B from their aqueous solution. J Hazard Mater. 2009;164:374–379.
[71] Santhi T, Prasad AL, Manonmani S. A comparative study of microwave and chemically treated Acacia nilotica leaf as an eco friendly adsorbent for the removal of Rhodamine B dye from aqueous solution. Arab J Chem. 2011;7:494–503. DOI: 10.1016/j.arabjc.2010.11.008.
[72] Chang S, Wang K, Li H, et al. Enhancement of Rhodamine B removal by low-cost fly ash sorption with Fenton pre-oxidation. J Hazard Mater. 2009;172:1131–1136.
[73] Chieng HI, Lim LBL, Priyantha N. Sorption characteristics of peat from Brunei Darussalam for the removal of rhodamine B dye from aqueous solution: adsorption isotherms, thermodynamics, kinetics and regeneration studies. Desalin Water Treat. 2015;55(3):664–677.
[74] Bello OS, Tan TS, Ahmad MA. Adsorption of remazol brilliant violet-5R reactive dye from aqueous solution by cocoa pod husk-based activated carbon: kinetic, equilibrium and thermodynamic studies. Asia Pac J Chem Eng. 2012;7:378–388.
[75] Dogan M, Ozdemir Y, Alkan M. Adsorption kinetics and mechanism of cationic methyl violet and methylene blue dyes onto sepiolite. Dyes Pigm. 2007;75:701–713.
[76] Gerçel O, Ozcan A, Ozcan AS, et al. Preparation of activated carbon from a renewable bio-plant of Euphorbia rigida by H_2SO_4 activation and its adsorption behavior in aqueous solutions. Appl Surf Sci. 2007;253:4843–4852.
[77] Wu FC, Tseng RI, Jung RS. Kinetic modeling of liquid-phase adsorption of reactive dyes and metal ions on chitosan. Water Res. 2001;35:613–618.
[78] Venkata S, Mohan N, Rao C, et al. Adsorptive removal of direct azo dye from aqueous phase onto coal based sorbents: a kinetic and mechanistic study. J Hazard Mater. 2002;90:189–204.
[79] Yang X, Al-Duri B. Kinetic modeling of liquid-phase adsorption of reactive dyes on activated carbon. J Colloid Interface Sci. 2005;287:25–34.
[80] Vimonses V, Lei S, Jin B, et al. Kinetic study and equilibrium isotherm analysis of Congo red adsorption by clay materials. Chem Eng J. 2009;148(2–3):354–364.
[81] Ozcan AS, Erdem B, Ozcan A. Adsorption of Acid Blue 193 from aqueous solutions onto BTMA-bentonite. Colloid Surf A Phys Eng Asp. 2005;266:73–81.
[82] Namasivayam C, Kavitha D. Removal of Congo Red from water by adsorption onto activated carbon prepared from coir pith, an agricultural solid waste. Dyes Pigm. 2002;54:47–58.
[83] Tan IAW, Ahmad AL, Hameed BH. Adsorption of basic dye using activated carbon prepared from oil palm shell: batch and fixed bed studies. Desalination. 2008;225:13–28.